NEUROLOGY

Imaging synaptic density in the living human brain

Sjoerd J. Finnema,[1]* Nabeel B. Nabulsi,[1] Tore Eid,[2] Kamil Detyniecki,[3] Shu-fei Lin,[1] Ming-Kai Chen,[1] Roni Dhaher,[2] David Matuskey,[1] Evan Baum,[1] Daniel Holden,[1] Dennis D. Spencer,[4] Joël Mercier,[5] Jonas Hannestad,[5†] Yiyun Huang,[1] Richard E. Carson[1,6]

Chemical synapses are the predominant neuron-to-neuron contact in the central nervous system. Presynaptic boutons of neurons contain hundreds of vesicles filled with neurotransmitters, the diffusible signaling chemicals. Changes in the number of synapses are associated with numerous brain disorders, including Alzheimer's disease and epilepsy. However, all current approaches for measuring synaptic density in humans require brain tissue from autopsy or surgical resection. We report the use of the synaptic vesicle glycoprotein 2A (SV2A) radioligand [^{11}C]UCB-J combined with positron emission tomography (PET) to quantify synaptic density in the living human brain. Validation studies in a baboon confirmed that SV2A is an alternative synaptic density marker to synaptophysin. First-in-human PET studies demonstrated that [^{11}C]UCB-J had excellent imaging properties. Finally, we confirmed that PET imaging of SV2A was sensitive to synaptic loss in patients with temporal lobe epilepsy. Thus, [^{11}C]UCB-J PET imaging is a promising approach for in vivo quantification of synaptic density with several potential applications in diagnosis and therapeutic monitoring of neurological and psychiatric disorders.

INTRODUCTION

The human brain is estimated to contain 100 trillion synapses (*1*). Structural disruption or loss of synapses can result in network dysfunction with aberrant neuronal signaling. Synaptic pathology has been associated with many brain disorders. Reduced synaptic density in the seizure onset zone in patients with epilepsy has been shown in neuropathological studies (*2*–*5*), and synapse loss in the hippocampus and cerebral cortex has been closely associated with cognitive impairment in Alzheimer's disease (*6*–*9*). Moreover, regional synaptic changes have been demonstrated in patients with autism (*10*), depression (*11*), or schizophrenia (*12*, *13*). However, all approaches for synapse quantification in humans depend on examination of brain tissue from autopsy or surgical resection, thereby greatly limiting the utility of this approach for early diagnosis and therapeutic monitoring. A minimally invasive method for quantification of synaptic density in the living human brain is therefore desired.

Quantification of synaptic density in brain tissue is typically performed using immunohistochemistry or electron microscopy. Antibodies targeting key proteins located in the pre- or postsynaptic neurons, such as synaptophysin (SYN), which is present in the membrane of synaptic vesicles (*14*), are commonly used for immunohistochemical detection of synaptic elements. In vivo quantification of proteins in the living brain is possible using positron emission tomography (PET), and the use of PET imaging is well established for a wide range of brain receptors, transporters, and enzymes, as well as other proteins (*15*). In vivo quantification of synapses throughout the entire brain may be possible using PET when combined with a synapse-specific radioligand, but to date, no radioligands have been reported that bind to a protein ubiquitously present on synaptic vessels. To this end, we developed [^{11}C]UCB-J [(*R*)-1-((3-(^{11}C-methyl-^{11}C)pyridin-4-yl)methyl)-4-(3,4,5-trifluorophenyl)pyrrolidin-2-one] as a best-in-class PET radioligand for imaging of the synaptic vesicle glycoprotein 2A (SV2A) and demonstrated its potential in nonhuman primates (*16*).

SV2 is present in all vertebrates and is an integral membrane protein located similarly to SYN in the presynaptic vesicle membranes. SV2 consists of three isoforms, with SV2A as the only isoform ubiquitously and homogeneously located in synapses across the brain (*17*). Thus, PET imaging and quantification of SV2A signal may be an excellent in vivo proxy of synaptic density. Other SV2A radioligands have been reported recently, including [^{11}C]UCB-A and [^{18}F]UCB-H (*18*). [^{11}C]UCB-A binding could be quantified in rats and pigs (*19*). [^{18}F]UCB-H displayed good kinetics in rats (*20*) and nonhuman primates (*21*), and acceptable dosimetry in humans (*22*), but a human brain imaging study has not yet been reported.

Here, we demonstrate that [^{11}C]UCB-J binds to SV2A and serves as a synaptic density marker in nonhuman primates as well as in people, in a first-in-human imaging study in healthy controls and in patients with epilepsy. In healthy humans, we characterized the pharmacokinetic and imaging properties of [^{11}C]UCB-J and confirmed SV2A-specific binding. We also demonstrated proof of concept in epilepsy patients that changes in synaptic density can be monitored noninvasively. [^{11}C]UCB-J PET is a promising approach for research, clinical diagnosis, and therapeutic monitoring in neurological and psychiatric disorders.

RESULTS

SV2A is a marker of synaptic density—A baboon case study

To validate [^{11}C]UCB-J as a marker of synaptic density, we performed a PET measurement in an olive baboon (*Papio anubis*), after which the animal was sacrificed and the brain was dissected for postmortem tissue studies. After injection of [^{11}C]UCB-J, brain uptake was rapid, with highest radioactivity concentrations in the cerebral cortex and lowest in the white matter region centrum semiovale (Fig. 1, A and B). Regional time-activity curves (TACs) displayed rapid kinetics, with peak uptake of

[1]Yale Positron Emission Tomography Center, Department of Radiology and Biomedical Imaging, Yale University, New Haven, CT 06520, USA. [2]Department of Laboratory Medicine, Yale University, New Haven, CT 06520, USA. [3]Department of Neurology, Yale University, New Haven, CT 06520, USA. [4]Department of Neurosurgery, Yale University, New Haven, CT 06520, USA. [5]UCB Pharma, B-1420 Braine-l'Alleud, Belgium. [6]Department of Biomedical Engineering, Yale University, New Haven, CT 06520, USA.
*Corresponding author. Email: sjoerd.finnema@yale.edu
†Present address: Denali Therapeutics, South San Francisco, CA 94080, USA.

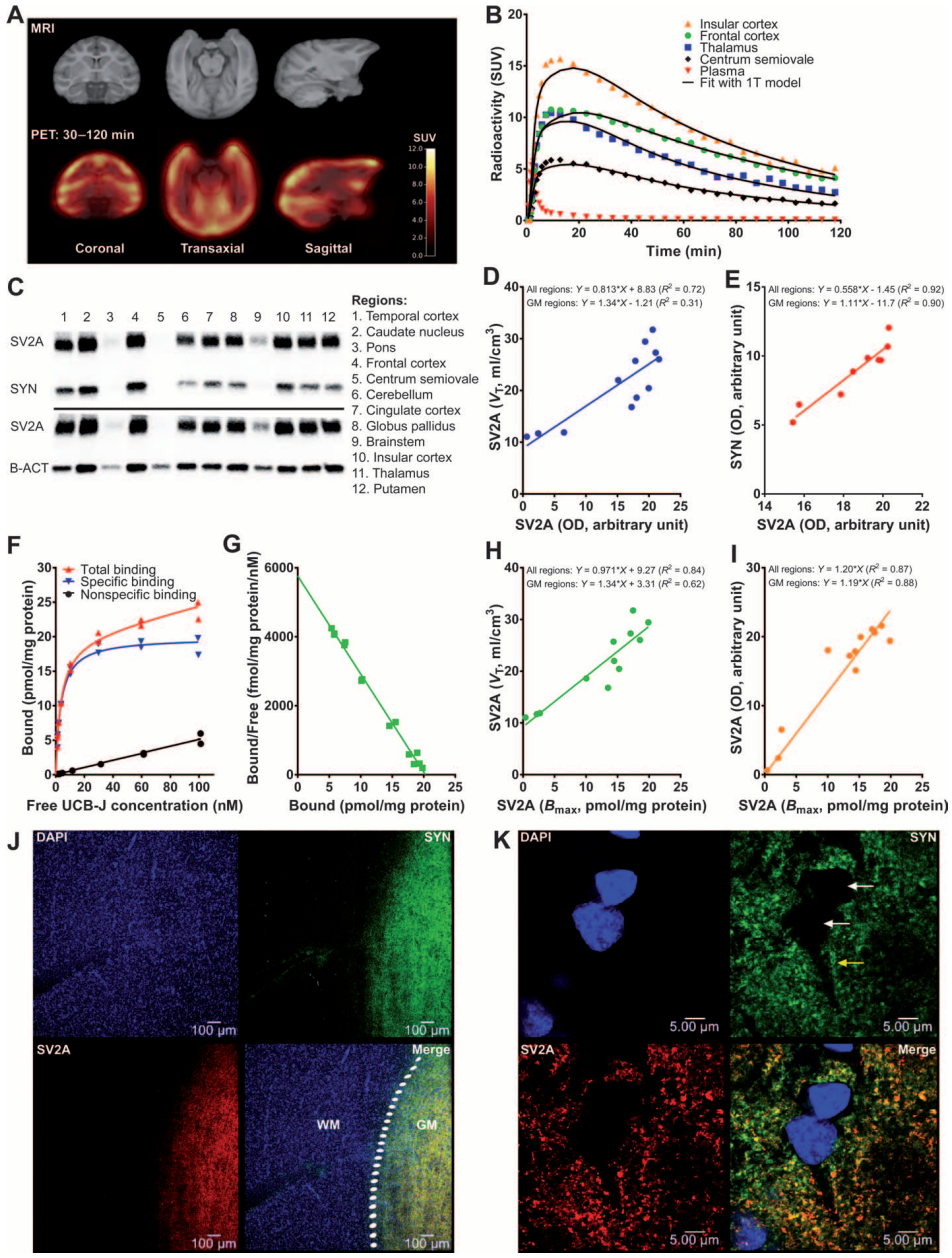

Fig. 1. In vivo–in vitro validation of [^{11}C]UCB-J as a synaptic density biomarker in the baboon brain. (**A**) Template MRI and PET summation images of baboon brain 30 to 120 min after intravenous injection of [^{11}C]UCB-J. (**B**) TACs of regional brain radioactivity in the insular cortex, frontal cortex, thalamus, and centrum semiovale and [^{11}C]UCB-J plasma concentration. The solid lines show curve fitting with the 1T compartment model. (**C**) Western blot analyses of 12 baboon brain regions. Western blot was performed with a polyclonal anti-SV2A antibody (83 kD; top and bottom), a monoclonal anti-SYN antibody (38 kD; top), and a monoclonal anti–β-actin antibody (42 kD; bottom). For each brain region, individual wells were loaded with 2 µg of protein. (**D**) Correlation between regional in vitro SV2A [optical density (OD) by Western blot] and in vivo SV2A (V_T by PET measures). Data are 12 brain regions. (**E**) Correlation between in vitro SV2A and in vitro SYN density in gray matter regions determined using Western blot analyses. Data are nine brain regions. (**F**) Saturation studies of [^{11}C]UCB-J were performed for 12 brain regions. Data are for the temporal cortex (each measurement was performed in duplicate), with 11 other regions in fig. S1. Membranes were incubated with increasing concentrations of UCB-J for 30 min at 37°C. Nonspecific binding was determined as the residual binding measured in the presence of 1 mM levetiracetam. Specific binding was determined by subtraction of the nonspecific from the total binding. (**G**) Scatchard plot from the transformed data of the temporal cortex in (F). Eleven other regions are shown in fig. S2. (**H**) Correlation between regional SV2A density (B_{max}) measured in vitro using tissue homogenate binding and regional [^{11}C]UCB-J binding measured in vivo in a baboon using PET. Data are 12 brain regions. (**I**) Correlation between regional SV2A density (B_{max}) measured in vitro using tissue homogenate binding and SV2A density using in vitro Western blot analyses (OD). Data are 12 brain regions. (**J**) Low-power confocal microscopy imaging of 4′,6-diamidino-2-phenylindole (DAPI), SYN, and SV2A in white matter and cortical gray matter in baboon brain. The dotted white line indicates the border between the white matter (WM; left) and the gray matter (GM; right). (**K**) High-power confocal microscopy of DAPI, SYN, and SV2A in the gray matter of the baboon brain from (J). Labeling for SYN and SV2A is evident as punctate staining in the neuropil, particularly surrounding neuronal cell bodies and proximal dendrites (yellow arrow), but absent in neuronal cell bodies (white arrows). Nuclei are indicated by the DAPI stain in blue.

10 to 15 [standardized uptake value (SUV); activity normalized to injection dose and body weight] in gray matter regions achieved within 6 to 16 min after injection. Regional volume of distribution (V_T) values, a measure of equilibrium binding, were estimated with the one-tissue (1T) compartment model and were in accordance with previously reported V_T values in five rhesus monkeys ($V_{T\ rhesus} = 1.86 \times V_{T\ baboon} - 0.0123$; $R^2 = 0.87$) (*16*).

Tissues were sampled from 12 regions in the baboon's brain and analyzed by Western blotting and SV2A homogenate binding assays. To determine whether SV2A can, like the gold standard SYN, be used as a marker of synaptic density, we compared regional densities of SV2A and SYN using selective antibodies for SV2A, SYN, and the housekeeping protein β-actin. SV2A and SYN signals were strong and specific in all gray matter regions but absent or weak in the centrum semiovale (Fig. 1C). The in vitro regional distribution of SV2A [optical density (OD)] correlated well with in vivo PET-measured [^{11}C]UCB-J V_T (Fig. 1D). There was an excellent linear correlation between SV2A and the "gold standard" synaptic marker SYN across all gray matter regions analyzed (Fig. 1E), indicating that SV2A can be used as an alternative to SYN for accurate synapse quantification.

To further evaluate the relationship between in vivo [^{11}C]UCB-J binding and SV2A density, homogenate binding studies were performed to determine affinity (K_d) and regional SV2A densities (B_{max}). Saturation studies using [^{11}C]UCB-J were conducted for 12 brain regions in a competition binding assay. [^{11}C]UCB-J bound with an average K_d of 3.9 ± 0.6 nM (±SD, $n = 11$) to a homogeneous population of binding sites, as illustrated in the temporal cortex, the region with the highest SV2A density (Fig. 1, F and G); 11 other regions of the brain are shown in figs. S1 and S2. The regional SV2A B_{max} ranged from 2.2 pmol/mg protein (111 pmol/ml brain tissue) in the pons to 19.9 pmol/mg protein (918 pmol/ml brain tissue) in the temporal cortex; specific binding could not be reliably detected in the centrum semiovale. The in vitro B_{max} values also correlated well with the in vivo V_T values measured in baboon (Fig. 1H). There was excellent correlation between the in vitro B_{max} derived from homogenate binding and the regional SV2A Western blot measurements (Fig. 1I).

To evaluate the cellular distribution of SV2A, we compared the localization of SV2A and SYN using selective antibodies. Immunoreactivity was evaluated in a section of the somatosensory cortex and the adjacent white matter using confocal microscopy (Fig. 1, J and K). There was considerable overlap between the staining for SYN and SV2A. SV2A and SYN staining was negligible in the white matter but high in the gray matter (Fig. 1J). SV2A and SYN staining was absent in neuronal cell bodies (white arrows in Fig. 1K) but high at the border of a proximal dendrite (yellow arrow in Fig. 1K). These data further support SV2A as an alternative to SYN for synapse quantification.

[^{11}C]UCB-J is a promising radioligand in humans

Five healthy subjects (37 ± 13 years of age; four males and one female) were evaluated with PET after an intravenous bolus injection of [^{11}C]UCB-J. All subjects underwent arterial cannulation, and blood was collected for measurement of the time course of [^{11}C]UCB-J in plasma, including radiometabolite analysis. Radio-HPLC (high-pressure liquid chromatography) analysis of the plasma demonstrated three radioactive peaks eluting between 6 and 8 min, with the [^{11}C]UCB-J fraction eluting at 11 min, comparable to monkey results (*16*). The unchanged [^{11}C]UCB-J fraction was 38 ± 16% (±SD) at 15 min after injection and further decreased to 25 ± 10% at 90 min after injection (table S1). The plasma free fraction of [^{11}C]UCB-J in a blood sample taken just before radioligand injection was 32 ± 0.7% (±SD) (table S2).

PET summation images in representative subject 1 demonstrated high radioactivity concentrations in all gray matter regions and low uptake in white matter regions (Fig. 2A; all other subjects, fig. S3) similar to the baboon. [^{11}C]UCB-J had peak SUV of 7 to 11 across gray matter brain regions at 10 to 25 min after injection, and the centrum semiovale showed considerably lower uptake than all examined gray matter regions in subject 1 (Fig. 2B; all other subjects, fig. S4). For all subjects, [^{11}C]UCB-J displayed favorable kinetics in all gray matter regions, with a steady decline in regional radioactivity over time, starting ~20 min after injection.

Kinetic analysis provided measures of both SV2A binding (V_T and BP_{ND}) and blood flow (K_1). Regional V_T values were estimated using the 1T model, which provided suitable fits for the TACs and reliable estimates of the V_T values (Fig. 2B). V_T values ranged from 5.2 ± 0.5 ml/cm^3 in the centrum semiovale to 22.5 ± 2.0 ml/cm^3 in the putamen (Fig. 2C and table S3). The coefficient of variation for V_T was 9 ± 3% across the examined brain regions, indicating a low intersubject variability. The K_1 values, determined from the 1T model and reflecting blood flow and tracer extraction, were heterogeneous across brain regions and ranged from 0.123 ± 0.017 ml/cm^3 per minute in the centrum semiovale to 0.376 ± 0.048 ml/cm^3 per minute in the putamen (Fig. 2D and table S4). Regional binding potential (BP_{ND}) values equal the ratio of specific to nondisplaceable (free plus nonspecific) binding and were determined from the V_T values (Fig. 2C and table S3) as $V_{T,region}/V_{T,centrum\_semiovale} - 1$. BP_{ND} values ranged from 1.69 ± 0.29 in the hippocampus to 3.33 ± 0.37 in the putamen (Fig. 2E and table S5). The intersubject coefficient of variation for BP_{ND} was 12 ± 2%.

To confirm that [^{11}C]UCB-J binds specifically to SV2A, displacement studies were performed with the SV2A-selective anticonvulsant levetiracetam (*23*). Three additional healthy subjects (32 ± 9 years of age; one male and two females) underwent a bolus plus constant infusion scan with [^{11}C]UCB-J under baseline conditions. One of these subjects (30 years of age; female) and two additional healthy subjects (35 and 46 years of age; two males) underwent a displacement measurement in which 1500-mg levetiracetam was administered intravenously 60 to 65 min after the start of [^{11}C]UCB-J infusion. Regional V_T values reached equilibrium after about 40 min (Fig. 3A; individual subjects 6 to 8, fig. S5A). Levetiracetam substantially decreased binding of [^{11}C]UCB-J in SV2A-rich regions by 90 to 120 min (30 to 60 min after levetiracetam infusion) as shown in TACs (Fig. 3B; individual subjects 8 to 10, fig. S5B) and in PET images (subject 8 in Fig. 3C; all subjects, fig. S6). In the displacement study, mean V_T for the 90- to 120-min periods was 44% lower in gray matter regions and 12% lower in the centrum semiovale, when compared to mean V_T for the 90- to 120-min period measured under baseline conditions.

[^{11}C]UCB-J binding is reduced in the seizure onset zone of epilepsy subjects

To evaluate the sensitivity of [^{11}C]UCB-J binding to synaptic loss, [^{11}C]UCB-J binding was evaluated with PET in three patients with temporal lobe epilepsy (TLE) and mesial temporal sclerosis (52 ± 6 years of age; three males). BP_{ND} maps were generated with the simplified reference tissue model 2 (*24*) using the centrum semiovale as a reference brain region for nondisplaceable binding. In all three patients, the unilateral decrease in uptake in the hippocampus was ipsilateral to the mesial temporal sclerosis seen on magnetic resonance imaging (MRI) and visually evident in the BP_{ND} maps and regional TACs (Fig. 4, A to D). The unilateral

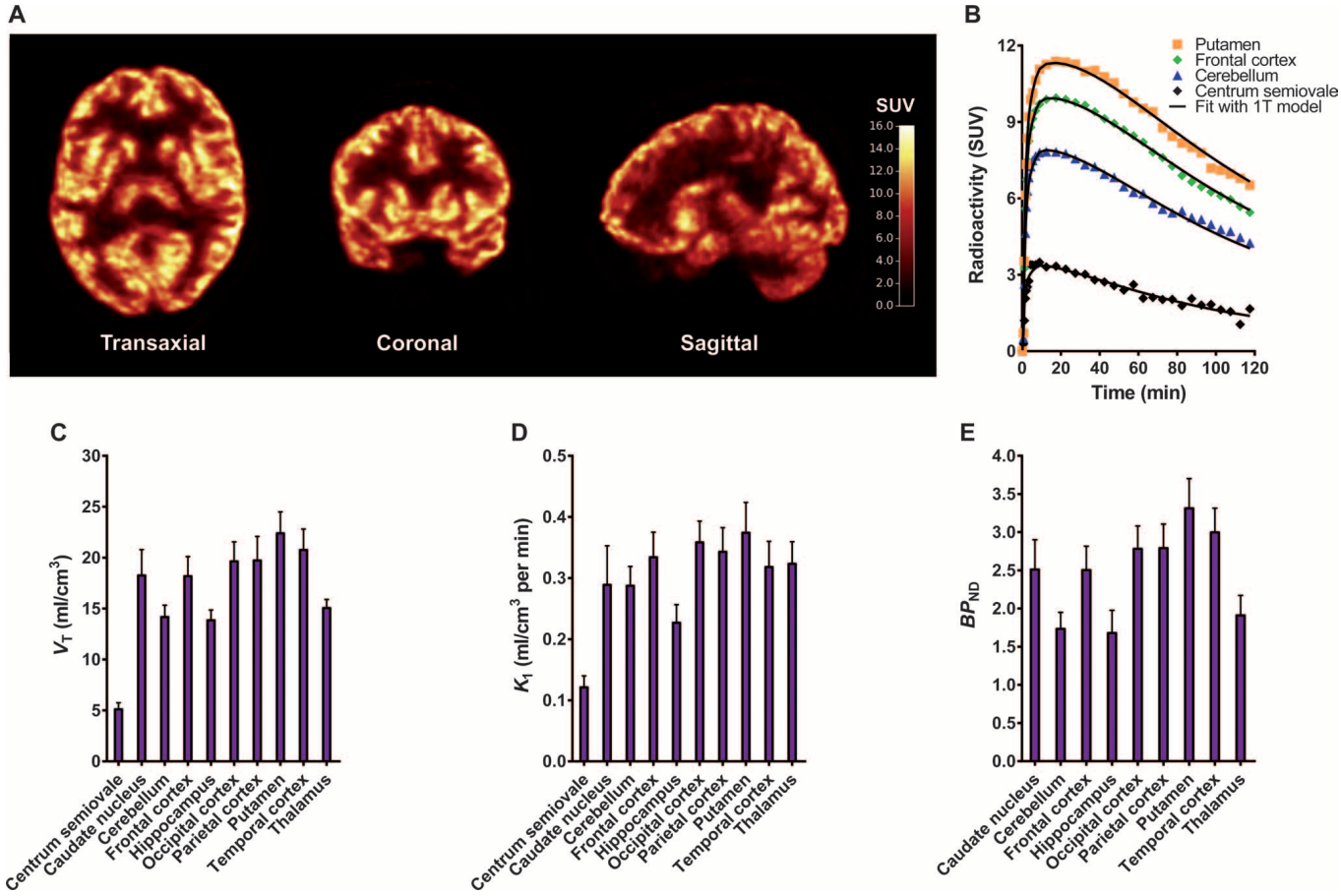

Fig. 2. PET imaging evaluation of SV2A-specific tracer [^{11}C]UCB-J in healthy human subjects. (**A**) PET summation images 40 to 60 min after [^{11}C]UCB-J injection in subject 1. Regional radioactivity was normalized to injected radioactivity and body weight and expressed as the SUV. Images for subjects 2 to 5 are shown in fig. S3. (**B**) TACs for regional brain radioactivity in putamen, frontal cortex, cerebellum, and centrum semiovale of subject 1. The solid lines show curve fitting with the 1T compartment model. Curves for subjects 2 to 5 are depicted in fig. S4. (**C**) Regional volumes of distribution (V_T) obtained by the 1T model applied to TACs. (**D**) Regional influx rate (K_1) values obtained by the 1T model applied to TACs. (**E**) BP_{ND} values. Data in (C) to (E) are means ± SD (n = 5). Individual subject values for V_T, K_1, and BP_{ND} are shown in tables S3 to S5.

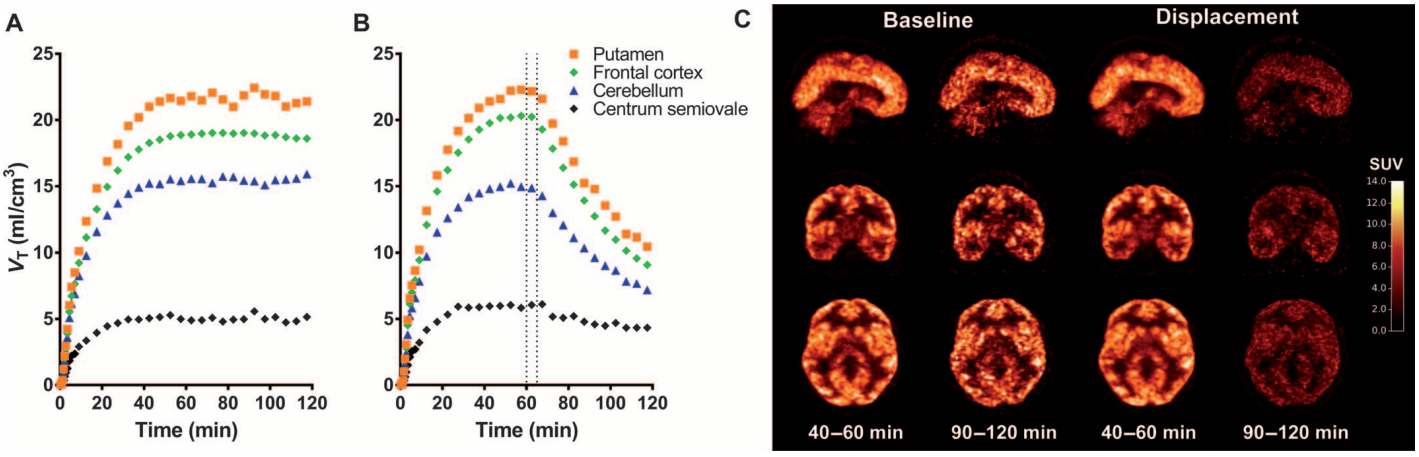

Fig. 3. [^{11}C]UCB-J binds to SV2A in the healthy human brain. (**A** and **B**) Regional TACs of V_T values in four brain regions after [^{11}C]UCB-J administration by a bolus plus constant infusion protocol in three control subjects under baseline (A) or displacement conditions in which levetiracetam (1500 mg) was intravenously infused 60 to 65 min after the start of [^{11}C]UCB-J infusion (B). Data are means (n = 3); the SD was not displayed for the sake of clarity. Individual subject data are shown in fig. S5. (**C**) PET summation images 40 to 60 min or 90 to 120 min after [^{11}C]UCB-J injection in subject 8. In the displacement study, levetiracetam (1500 mg) was intravenously infused 60 to 65 min after the start of [^{11}C]UCB-J infusion. Individual subject images are shown in fig. S6.

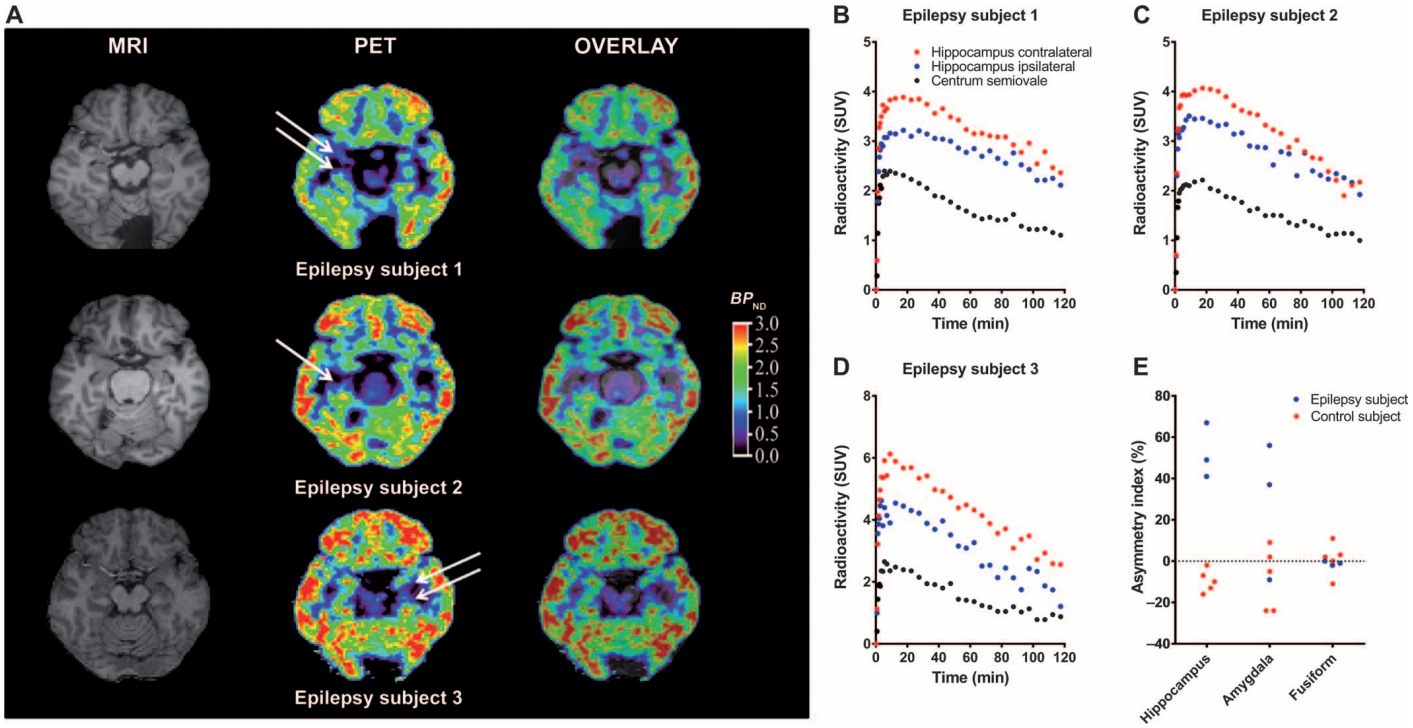

Fig. 4. PET evaluation with [^{11}C]UCB-J reveals unilateral mesial temporal sclerosis in epilepsy patients. (**A**) MR images, corresponding BP_{ND} maps of [^{11}C]UCB-J, and overlay in three TLE patients with unilateral mesial temporal sclerosis. The white arrows indicate loss of [^{11}C]UCB-J binding in the mesial temporal lobe. (**B** to **D**) Regional TACs for radioactivity in hippocampus and centrum semiovale after intravenous injection of [^{11}C]UCB-J in three epilepsy subjects. (**E**) Asymmetry indices between left and right hemispheres for healthy control subjects and between ipsilateral and contralateral hemispheres for epilepsy patients. Data are individual subjects, including original control subjects 1 to 5.

uptake of [^{11}C]UCB-J was region-specific, with no asymmetry observed in the fusiform (Fig. 4E). Regional asymmetry indices factoring in contralateral versus ipsilateral SV2A density were much higher in the hippocampus and amygdala of epilepsy patients than bilateral asymmetry in healthy subjects (Fig. 4E). In two epilepsy patients, in addition to hippocampal synapse loss, there was asymmetry in the amygdala, consistent with previous reports that damage in the amygdala is present in a significant subpopulation of TLE patients (*25*).

DISCUSSION

The number of synapses in the brain changes over the course of a lifetime, and synaptogenesis, synaptic pruning, and synaptic degeneration are key physiologic and pathologic processes regulating synaptic density (*26*). Evaluation of synaptic density in humans has been limited to examination of brain tissue obtained from surgery or autopsy. However, quantification of synaptic densities in the living human brain over time is essential to our understanding, diagnosis, and treatment of brain disorders associated with synaptic pathology. Here, we presented a noninvasive method for PET imaging and quantification of synaptic density throughout the brain using the radioligand [^{11}C]UCB-J for the target SV2A—a synaptic vesicles marker that, in one baboon brain, was shown to localize with the accepted marker SYN. In humans, [^{11}C]UCB-J bound to SV2A in the brain and revealed unilateral synaptic loss in TLE patients. Thus, SV2A-PET imaging is a promising approach for quantifying synaptic density in the living human brain.

The restricted cellular localization of vesicles in synaptic boutons, their ubiquitous distribution in the brain, and high phylogenetic conservation across vertebrate nervous systems have made synaptic vesicle proteins the prime markers of synaptic density (*27*–*30*). SYN is the most abundant synaptic vesicle protein (*31*) and is a widely used marker of synaptic density (*32*, *33*), because it was one of the first characterized (*29*, *34*) and cloned (*35*) vesicle membrane proteins. In the baboon case study, we demonstrated that the cellular and regional distributions of SV2A and SYN were highly correlated, suggesting that SV2A is a valid alternative synaptic density marker. Although SYN is the most polydispersed vesicle protein, possibly reflecting its variability among the vesicles of different neurotransmitter classes, SV2A is the most monodispersed synaptic vesicle protein (*36*). Consequently, SV2A may provide a more accurate measure of synaptic density owing to its greater uniformity in vesicles. The relevance of SV2A as a synaptic marker was recently exemplified in a study in which the FYN tyrosine kinase inhibitor AZD0530 rescued both memory and synapse (SV2A) loss in a mouse model of Alzheimer's disease (*37*).

Unlike other human imaging technologies, such as MRI, PET imaging is quantitative and provides outcome measures directly related to protein concentrations that can be cross-validated in animals or postmortem tissues. For example, V_T, one PET-derived outcome measure, is proportional to the ratio of protein density (B_{max}) and binding affinity (K_d) (*38*). No detailed regional densities of SV2A were available in the literature. However, in vitro SV2A densities were determined and found to correlate well with the in vivo PET V_T values. Mean cortical B_{max} values in baboon were 18 pmol/mg protein, somewhat higher than the values of 3 to 12 pmol/mg protein in rats (*39*, *40*) and 3 to 4 pmol/mg protein in

humans, but these differences are likely due to methodological dissimilarities in radioligand, isotope, incubation conditions, or tissue type, for instance. The estimated K_d for SV2A binding by UCB-J was similar to previously reported inhibition constant (K_i) values in human tissue (6 to 7 nM), further validating our results (*18*).

Saturation studies with PET can also provide estimates of in vivo B_{max} and K_d values (*41*). We recently determined the in vivo K_d value as 3.4 nM and cortical B_{max} values in the range of 300 to 400 nM with [^{11}C]UCB-J in rhesus monkeys (*16*), which corresponded well with the current in vitro results in baboon tissues. Thus, the SV2A density in the temporal cortex is estimated to be 5.5×10^{17} SV2A molecules per liter of brain tissue. Assuming a density of 7.2×10^{14} synapses per liter of brain tissue, as reported for the female human brain (*42*), and two to five SV2A copies per vesicle (*31*, *36*), it can be estimated that there are 154 to 385 vesicles per synapse. This number is very similar to the previously reported 200 to 350 vesicles per active zone in rat cultured hippocampal preparations, *Drosophila* neuromuscular junctions, or rat calyx of Held terminals, although other species have higher numbers of vesicles (*43*).

In patients with medically refractory TLE and concomitant mesial temporal sclerosis, in which unilateral loss of neurons is well established (*5*), we found ~52% asymmetry in the hippocampus owing to decreased binding of [^{11}C]UCB-J ipsilateral to the epileptogenic zone. This degree of reduction in [^{11}C]UCB-J binding corresponds well with previous tissue-level analyses, where SYN or SV2A was reported to be reduced by 30 to 60% in the anterior temporal neocortex or hippocampus in resected tissue from TLE patients in parallel with neuronal/synaptic loss (*2*–*5*). When comparing the asymmetry in [^{11}C]UCB-J binding to [^{18}F]FDG (2-deoxy-2-^{18}F-fluoro-D-glucose), a clinically established marker of glucose metabolism, asymmetry in [^{11}C]UCB-J binding was more specifically localized to the epileptogenic mesial temporal lobe, whereas [^{18}F]FDG hypometabolism usually extends to the lateral temporal lobe and other adjacent regions (*44*). The reductions in [^{11}C]UCB-J binding were also larger than those typically reported for [^{18}F]FDG (typically <20%), but these findings require confirmation, ideally by comparing both radioligands in the same subject. [^{11}C]UCB-J may thus provide accurate identification of the epileptogenic zone and have high utility in pharmacoresistant TLE patients in which surgery is frequently the only therapeutic possibility.

The current study has several limitations. The overall sample size was small; PET studies were performed in 13 subjects, and tissue experiments were performed using only one baboon. Also, it could not be concluded that the centrum semiovale is a suitable reference region for [^{11}C]UCB-J quantification. A reference tissue devoid of specific binding can be used as a substitute for arterial blood sampling. In our tissue measurements, we found that the centrum semiovale contained none or negligible SV2A (at least 45-fold lower than cortical regions). However, PET studies with levetiracetam suggested a small amount of displaceable [^{11}C]UCB-J binding in centrum semiovale. These preliminary results did not include correction for the partial volume effect (*45*), which causes spill-in of radioactivity from gray matter to white matter. Centrum semiovale therefore remains a promising reference region, and follow-up studies and analyses, including blocking studies in humans with other SV2A ligands, such as brivaracetam, will be required to validate the absence of SV2A-specific [^{11}C]UCB-J binding in this region.

To facilitate that translation of synaptic density imaging with SV2A-PET, it is important to review a number of methodological considerations. Evaluation of the TACs suggests that the outcome measure V_T can be reliably estimated using only a 60-min acquisition, which would improve patient comfort. Alternatively, using constant infusion can provide a very short imaging period during equilibrium. Notably, [^{11}C]UCB-J is radiolabeled with carbon-11, with a short half-life ($t_{1/2}$) of 20 min. However, diagnostic PET radioligands are typically labeled with fluorine-18 ($t_{1/2}$ = 110 min) to allow for distribution from production facilities to hospitals. Fortuitously, UCB-J contains three fluorine atoms and radiosynthesis of [^{18}F]UCB-J may thus be possible.

PET imaging of SV2A now provides the unique opportunity to evaluate synaptic density in the living human brain. Our in vitro and in vivo data support the hypothesis that SV2A-PET imaging can be used as a minimally invasive, quantitative marker of synaptic density. The radioligand [^{11}C]UCB-J has exceptional PET imaging qualities for SV2A in the human brain. We demonstrate feasibility in epilepsy, but the application of SV2A-PET imaging as a synaptic marker may be particularly relevant to Alzheimer's disease, in which the pathology is characterized by accumulation of misfolded proteins (plaques composed of amyloid β, and Tau-containing neurofibrillary tangles) and synaptic loss (*46*).

MATERIALS AND METHODS

Study design

The overall objective was a proof-of-concept study that SV2A-PET imaging could be a method for in vivo measurement of synaptic density. The size of the healthy control population (n = 10) was consistent with previous novel radioligand evaluation studies (*47*–*49*) and was chosen to demonstrate the imaging characteristics of the tracer, including kinetic analyses and determination of population values for the study end points (K_d, V_T, and BP_{ND}). The epilepsy patient population was chosen to demonstrate the presence of a large asymmetry in the temporal lobe. The number of epilepsy subjects was based on the small variability in the bilateral asymmetry index observed in the PET studies in healthy control subjects, and the large reduction in synaptic density in resected tissue from epilepsy subjects (*2*–*5*). All outliers were included in the analysis, and no data were excluded. No experimental groups were included in the study, and no randomization was required. The authors were not blinded to the results. We performed a terminal study in one baboon to directly compare in vivo/in vitro results of tracer binding to synaptic vesicles and localization in different brain regions; the selection of n = 1 was based on a conservative approach to terminal primate studies.

PET imaging and brain tissue measurements in a baboon

Experiments were conducted in one olive baboon (*P. anubis*) according to a protocol approved by the Yale University Institutional Animal Care and Use Committee, as described in Supplementary Methods.

Human subjects

Ten healthy subjects (seven males and three females; 36 ± 10 years of age) and three epilepsy subjects (three males; 52 ± 6 years of age) were included in the study. All epilepsy patients had medically refractory mesial TLE with hippocampal sclerosis and were undergoing presurgical evaluation. None of the epilepsy patients had received levetiracetam. The studies were performed under a protocol approved by the Yale University Human Investigation Committee and the Yale New Haven Hospital Radiation Safety Committee, and in accordance with the U.S. federal policy for the protection of human research subjects contained in Title 45 Part 46 of the Code of Federal Regulations (45 CFR 46). Written informed consent was obtained from all subjects. As part of the subject evaluation, MR images were acquired on all subjects to eliminate

subjects with structural brain abnormalities and for registration of PET images. MRI was performed on a 3-T whole-body scanner (Trio, Siemens Medical Solutions) with a circularly polarized head coil. The dimension and pixel size of MR images were 256 × 256 × 176 and 0.98 × 0.98 × 1.0 mm^3, respectively.

PET measurements in human subjects

[^{11}C]UCB-J was synthesized at the Yale PET Center as previously reported (*16*). All [^{11}C]UCB-J PET measurements were conducted on the High Resolution Research Tomograph (Siemens Medical Solutions), which acquires 207 slices (1.2-mm slice separation) with a reconstructed image resolution (full width at half maximum) of ~3 mm. Before every [^{11}C]UCB-J injection, a 6-min transmission scan was performed for attenuation correction. PET data were acquired in list mode for 120 min after the start of the [^{11}C]UCB-J administration. Five control subjects (subjects 1 to 5) and three epilepsy subjects underwent a PET scan after an intravenous bolus injection of [^{11}C]UCB-J over 1 min (by an automated infusion pump; Harvard PHD 22/2000, Harvard Apparatus). In five other control subjects (subjects 6 to 10), bolus plus infusion studies were performed, where the bolus was followed by a constant infusion to the end of the PET acquisition (*50*). In the bolus plus constant infusion studies, the applied K_{bol} value was 150 min, based on simulations using the regional TACs from the five healthy control subjects evaluated with PET after bolus injection of [^{11}C]UCB-J. Baseline measurements were performed in three subjects (subjects 6 to 8). In subject 8, a second PET displacement measurement with levetiracetam was performed on the same day. Two other subjects (subjects 9 and 10) only underwent a PET measurement with levetiracetam displacement. In the displacement PET measurement, 1500 mg of the anticonvulsant levetiracetam was intravenously infused over 5 min starting 60 min after the start of [^{11}C]UCB-J administration to assess specific binding.

The injected mass was limited to 10 μg of UCB-J. The injected dose of [^{11}C]UCB-J was 408 ± 179 MBq, with specific activity at the time of injection of 176 ± 101 MBq/nmol. The corresponding injected UCB-J mass was 3.7 ± 2.6 nmol or 15 ± 10 ng/kg.

The dynamic emission data were reconstructed into 33 frames (6 × 0.5, 3 × 1, 2 × 2, and 22 × 5 min) with corrections for attenuation, normalization, scatter, randoms, and dead time using the MOLAR algorithm (*51*). Event-by-event motion correction (*52*) was included in the reconstruction on the basis of motion detection with a Polaris Vicra optical tracking system (NDI Systems) using reflectors mounted on a swim cap worn by the subject.

Arterial input functions

Each subject underwent catheterization of the radial artery for blood sampling. Samples were drawn every 10 s for the first 90 s and at 1.75, 2, 2.25, 2.5, 2.75, 3, 4, 5, 6, 8, 10, 15, 20, 25, 30, 45, 60, 75, 90, 105, and 120 min after [^{11}C]UCB-J injection. For each sample, plasma was obtained by centrifugation at 4°C (2930*g* for 5 min). Whole blood and plasma were counted in cross-calibrated γ-counters (Wizard^2; PerkinElmer). Plasma samples at 3, 8, 15, 30, 60, and 90 min after [^{11}C]UCB-J injection were also analyzed for unmetabolized [^{11}C]UCB-J fraction. Metabolite analysis and free fraction of [^{11}C]UCB-J in plasma were determined as described in Supplementary Methods.

Image registration and definition of regions of interest

For each subject, the hardware motion-corrected dynamic PET data were coregistered to an early summed PET image (0 to 10 min after [^{11}C]UCB-J injection) using a six-parameter mutual information algorithm (FLIRT of FSL) to eliminate any residual motion. The summed PET image was coregistered to the subject's individual T1-weighted 3-T MR image (six-parameter rigid registration), which was subsequently coregistered to the automated anatomical labeling (AAL) template in the Montreal Neurological Institute (MNI) space using nonlinear transformation (BioImage Suite) (*53*). Regions of interest were taken from the AAL template for SPM2 in MNI space. Using the inverse combined transformations from template to PET space, we generated regional TACs for the amygdala, caudate nucleus, centrum semiovale, cerebellum, frontal cortex, fusiform, hippocampus, occipital cortex, parietal cortex, putamen, temporal cortex, and thalamus. Values are expressed in SUV (dimensionless) equal to the regional activity concentration (Bq/ml) normalized by the ratio of injected dose (kBq) to subject weight (kg).

Quantitative analysis of [^{11}C]UCB-J binding

Regional TACs were analyzed with kinetic models using the arterial plasma TAC as input function. The regional distribution volumes (V_T) (*38*) were calculated using the 1T compartment model as K_1/k_2. For bolus plus constant infusion studies, V_T was calculated as the ratio of tissue activity (from PET) to that in metabolite-corrected plasma. On the basis of the Western blot, homogenate binding, and confocal microscopy results, the centrum semiovale was used as a reference region for determination of nondisplaceable binding and BP_{ND} values. Regional BP_{ND} values were calculated as $V_{T,region}/V_{T,centrum\_semiovale} - 1$.

Parametric BP_{ND} maps were generated using the simplified reference tissue model 2 (*24*) and used for calculation of regional BP_{ND} values. Asymmetry indices in regional BP_{ND} values were calculated in healthy control as 200% × [(left − right)/(left + right)] and in epilepsy patients as 200% × [(contralateral − ipsilateral)/(contralateral + ipsilateral)]. All kinetic modeling was performed with in-house developed programs written with IDL 8.0 (ITT Visual Information Solutions). For parameter estimation, data points were weighted on the basis of noise equivalent counts in each frame.

SUPPLEMENTARY MATERIALS

www.sciencetranslationalmedicine.org/cgi/content/full/8/348/348ra96/DC1

Methods

Fig. S1. Saturation studies of [^{11}C]UCB-J in regions of the baboon brain.

Fig. S2. Scatchard plots of [^{11}C]UCB-J in regions of the baboon brain.

Fig. S3. PET summation images after bolus injection of [^{11}C]UCB-J in healthy human subjects.

Fig. S4. Regional TACs after bolus injection of [^{11}C]UCB-J in healthy human subjects.

Fig. S5. Regional TACs of V_T values after bolus plus constant infusion of [^{11}C]UCB-J in additional healthy human subjects.

Fig. S6. PET summation images after bolus plus constant infusion of [^{11}C]UCB-J in human subjects.

Table S1. Unchanged [^{11}C]UCB-J fraction in plasma in five control subjects evaluated with bolus injection of [^{11}C]UCB-J.

Table S2. Plasma free fraction of [^{11}C]UCB-J in five control subjects evaluated with bolus injection of [^{11}C]UCB-J.

Table S3. Regional V_T values after bolus injection of [^{11}C]UCB-J in five control subjects.

Table S4. Regional K_1 values after bolus injection of [^{11}C]UCB-J in five control subjects.

Table S5. BP_{ND} values after bolus injection of [^{11}C]UCB-J in five control subjects.

References (*54*–*57*)

REFERENCES AND NOTES

1. F. A. C. Azevedo, L. R. B. Carvalho, L. T. Grinberg, J. M. Farfel, R. E. L. Ferretti, R. E. P. Leite, W. Jacob Filho, R. Lent, S. Herculano-Houzel, Equal numbers of neuronal and nonneuronal

cells make the human brain an isometrically scaled-up primate brain. *J. Comp. Neurol.* **513**, 532–541 (2009).
2. G. Feng, F. Xiao, Y. Lu, Z. Huang, J. Yuan, Z. Xiao, Z. Xi, X. Wang, Down-regulation synaptic vesicle protein 2A in the anterior temporal neocortex of patients with intractable epilepsy. *J. Mol. Neurosci.* **39**, 354–359 (2009).
3. E. A. Van Vliet, E. Aronica, S. Redeker, K. Boer, J. A. Gorter, Decreased expression of synaptic vesicle protein 2A, the binding site for levetiracetam, during epileptogenesis and chronic epilepsy. *Epilepsia* **50**, 422–433 (2009).
4. J. Crèvecoeur, R. M. Kaminski, B. Rogister, P. Foerch, C. Vandenplas, M. Neveux, M. Mazzuferi, J. Kroonen, C. Poulet, D. Martin, B. Sadzot, E. Rikir, H. Klitgaard, G. Moonen, M. Deprez, Expression pattern of synaptic vesicle protein 2 (SV2) isoforms in patients with temporal lobe epilepsy and hippocampal sclerosis. *Neuropathol. Appl. Neurobiol.* **40**, 191–204 (2014).
5. E. A. Proper, A. B. Oestreicher, G. H. Jansen, C. W. M. v. Veelen, P. C. van Rijen, W. H. Gispen, P. N. E. de Graan, Immunohistochemical characterization of mossy fibre sprouting in the hippocampus of patients with pharmaco-resistant temporal lobe epilepsy. *Brain* **123**, 19–30 (2000).
6. S. T. DeKosky, S. W. Scheff, Synapse loss in frontal cortex biopsies in Alzheimer's disease: Correlation with cognitive severity. *Ann. Neurol.* **27**, 457–464 (1990).
7. R. D. Terry, E. Masliah, D. P. Salmon, N. Butters, R. DeTeresa, R. Hill, L. A. Hansen, R. Katzman, Physical basis of cognitive alterations in Alzheimer's disease: Synapse loss is the major correlate of cognitive impairment. *Ann. Neurol.* **30**, 572–580 (1991).
8. J. E. Hamos, L. J. DeGennaro, D. A. Drachman, Synaptic loss in Alzheimer's disease and other dementias. *Neurology* **39**, 355–361 (1989).
9. J. L. Robinson, L. Molina-Porcel, M. M. Corrada, K. Raible, E. B. Lee, V. M.-Y. Lee, C. H. Kawas, J. Q. Trojanowski, Perforant path synaptic loss correlates with cognitive impairment and Alzheimer's disease in the oldest-old. *Brain* **137**, 2578–2587 (2014).
10. G. Tang, K. Gudsnuk, S.-H. Kuo, M. L. Cotrina, G. Rosoklija, A. Sosunov, M. S. Sonders, E. Kanter, C. Castagna, A. Yamamoto, Z. Yue, O. Arancio, B. S. Peterson, F. Champagne, A. J. Dwork, J. Goldman, D. Sulzer, Loss of mTOR-dependent macroautophagy causes autistic-like synaptic pruning deficits. *Neuron* **83**, 1131–1143 (2014).
11. H. J. Kang, B. Voleti, T. Hajszan, G. Rajkowska, C. A. Stockmeier, P. Licznerski, A. Lepack, M. S. Majik, L. S. Jeong, M. Banasr, H. Son, R. S. Duman, Decreased expression of synapse-related genes and loss of synapses in major depressive disorder. *Nat. Med.* **18**, 1413–1417 (2012).
12. L. A. Glantz, D. A. Lewis, Decreased dendritic spine density on prefrontal cortical pyramidal neurons in schizophrenia. *Arch. Gen. Psychiatry* **57**, 65–73 (2000).
13. A. Sekar, A. R. Bialas, H. de Rivera, A. Davis, T. R. Hammond, N. Kamitaki, K. Tooley, J. Presumey, M. Baum, V. Van Doren, G. Genovese, S. A. Rose, R. E. Handsaker; Schizophrenia Working Group of the Psychiatric Genomics Consortium, M. J. Daly, M. C. Carroll, B. Stevens, S. A. McCarroll, Schizophrenia risk from complex variation of complement component 4. *Nature* **530**, 177–183 (2016).
14. K. Buckley, R. B. Kelly, Identification of a transmembrane glycoprotein specific for secretory vesicles of neural and endocrine cells. *J. Cell Biol.* **100**, 1284–1294 (1985).
15. T. Jones, E. A. Rabiner, The development, past achievements, and future directions of brain PET. *J. Cereb. Blood Flow Metab.* **32**, 1426–1454 (2012).
16. N. B. Nabulsi, J. Mercier, D. Holden, S. Carré, S. Najafzadeh, M.-C. Vandergeten, S.-f. Lin, A. Deo, N. Price, M. Wood, T. Lara-Jaime, F. Montel, M. Laruelle, R. E. Carson, J. Hannestad, Y. Huang, Synthesis and preclinical evaluation of ^{11}C-UCB-J as a PET tracer for imaging the synaptic vesicle glycoprotein 2A in the brain. *J. Nucl. Med.* **57**, 777–784 (2016).
17. S. M. Bajjalieh, G. D. Frantz, J. M. Weimann, S. K. McConnell, R. H. Scheller, Differential expression of synaptic vesicle protein 2 (SV2) isoforms. *J. Neurosci.* **14**, 5223–5235 (1994).
18. J. Mercier, L. Archen, V. Bollu, S. Carré, Y. Evrard, E. Jnoff, B. Kenda, B. Lallemand, P. Michel, F. Montel, F. Moureau, N. Price, Y. Quesnel, X. Sauvage, A. Valade, L. Provins, Discovery of heterocyclic nonacetamide synaptic vesicle protein 2A (SV2A) ligands with single-digit nanomolar potency: Opening avenues towards the first SV2A positron emission tomography (PET) ligands. *ChemMedChem* **9**, 693–698 (2014).
19. S. Estrada, M. Lubberink, A. Thibblin, M. Sprycha, T. Buchanan, N. Mestdagh, B. Kenda, J. Mercier, L. Provins, M. Gillard, D. Tytgat, G. Antoni, [^{11}C]UC-A, a novel PET tracer for synaptic vesicle protein 2A. *Nucl. Med. Biol.* **43**, 325–332 (2016).
20. G. I. Warnock, J. Aerts, M. A. Bahri, F. Bretin, C. Lemaire, F. Giacomelli, F. Mievis, N. Mestdagh, T. Buchanan, A. Valade, J. Mercier, M. Wood, M. Gillard, A. Seret, A. Luxen, E. Salmon, A. Plenevaux, Evaluation of ^{18}F-UCB-H as a novel PET tracer for synaptic vesicle protein 2A in the brain. *J. Nucl. Med.* **55**, 1336–1341 (2014).
21. M.-Q. Zheng, D. Holden, N. Nabulsi, S.-f. Lin, J. Mercier, J. Hannestad, M. Laruelle, R. Carson, Y. Huang, Synthesis and evaluation of ^{18}F-UCB-H, a novel PET imaging tracer for the synaptic vesicle protein 2A. *J. Nucl. Med.* **55**, 1792 (2014).
22. F. Bretin, M. A. Bahri, C. Bernard, G. Warnock, J. Aerts, N. Mestdagh, T. Buchanan, C. Otoul, F. Koestler, F. Mievis, F. Giacomelli, C. Degueldre, R. Hustinx, A. Luxen, A. Seret, A. Plenevaux, E. Salmon, Biodistribution and radiation dosimetry for the novel SV2A radiotracer [^{18}F]UCB-H: First-in-human study. *Mol. Imaging Biol.* **17**, 557–564 (2015).
23. H. Klitgaard, P. Verdru, Levetiracetam: The first SV2A ligand for the treatment of epilepsy. *Expert Opin. Drug Discov.* **2**, 1537–1545 (2007).
24. Y. Wu, R. E. Carson, Noise reduction in the simplified reference tissue model for neuroreceptor functional imaging. *J. Cereb. Blood Flow Metab.* **22**, 1440–1452 (2002).
25. V. Aroniadou-Anderjaska, B. Fritsch, F. Qashu, M. F. M. Braga, Pathology and pathophysiology of the amygdala in epileptogenesis and epilepsy. *Epilepsy Res.* **78**, 102–116 (2008).
26. P. Rakic, J. P. Bourgeois, P. S. Goldman-Rakic, Synaptic development of the cerebral cortex: Implications for learning, memory, and mental illness. *Prog. Brain Res.* **102**, 227–243 (1994).
27. S. E. Goelz, E. J. Nestler, B. Chehrazi, P. Greengard, Distribution of protein I in mammalian brain as determined by a detergent-based radioimmunoassay. *Proc. Natl. Acad. Sci. U.S.A.* **78**, 2130–2134 (1981).
28. E. Perdahl, R. Adolfsson, I. Alafuzoff, K. A. Albert, E. J. Nestler, P. Greengard, B. Winblad, Synapsin I (protein I) in different brain regions in senile dementia of Alzheimer type and in multi-infarct dementia. *J. Neural Transm.* **60**, 133–141 (1984).
29. F. Navone, R. Jahn, G. Di Gioia, H. Stukenbrok, P. Greengard, P. De Camilli, Protein p38: An integral membrane protein specific for small vesicles of neurons and neuroendocrine cells. *J. Cell Biol.* **103**, 2511–2527 (1986).
30. P. De Camilli, S. M. Harris Jr., W. B. Huttner, P. Greengard, Synapsin I (Protein I), a nerve terminal-specific phosphoprotein. II. Its specific association with synaptic vesicles demonstrated by immunocytochemistry in agarose-embedded synaptosomes. *J. Cell Biol.* **96**, 1355–1373 (1983).
31. S. Takamori, M. Holt, K. Stenius, E. A. Lemke, M. Grønborg, D. Riedel, H. Urlaub, S. Schenck, B. Brügger, P. Ringler, S. A. Müller, B. Rammner, F. Gräter, J. S. Hub, B. L. De Groot, G. Mieskes, Y. Moriyama, J. Klingauf, H. Grubmüller, J. Heuser, F. Wieland, R. Jahn, Molecular anatomy of a trafficking organelle. *Cell* **127**, 831–846 (2006).
32. E. Masliah, R. D. Terry, M. Alford, R. De Teresa, Quantitative immunohistochemistry of synaptophysin in human neocortex: An alternative method to estimate density of presynaptic terminals in paraffin sections. *J. Histochem. Cytochem.* **38**, 837–844 (1990).
33. P. Knaus, H. Betz, H. Rehm, Expression of synaptophysin during postnatal development of the mouse brain. *J. Neurochem.* **47**, 1302–1304 (1986).
34. B. Wiedenmann, W. W. Franke, Identification and localization of synaptophysin, an integral membrane glycoprotein of M_r 38,000 characteristic of presynaptic vesicles. *Cell* **41**, 1017–1028 (1985).
35. R. E. Leube, P. Kaiser, A. Seiter, R. Zimbelmann, W. W. Franke, H. Rehm, P. Knaus, P. Prior, H. Betz, H. Reinke, K. Beyreuther, B. Wiedenmann, Synaptophysin: Molecular organization and mRNA expression as determined from cloned cDNA. *EMBO J.* **6**, 3261–3268 (1987).
36. S. A. Mutch, P. Kensel-Hammes, J. C. Gadd, B. S. Fujimoto, R. W. Allen, P. G. Schiro, R. M. Lorenz, C. L. Kuyper, J. S. Kuo, S. M. Bajjalieh, D. T. Chiu, Protein quantification at the single vesicle level reveals that a subset of synaptic vesicle proteins are trafficked with high precision. *J. Neurosci.* **31**, 1461–1470 (2011).
37. A. C. Kaufman, S. V. Salazar, L. T. Haas, J. Yang, M. A. Kostylev, A. T. Jeng, S. A. Robinson, E. C. Gunther, C. H. van Dyck, H. B. Nygaard, S. M. Strittmatter, Fyn inhibition rescues established memory and synapse loss in Alzheimer mice. *Ann. Neurol.* **77**, 953–971 (2015).
38. R. B. Innis, V. J. Cunningham, J. Delforge, M. Fujita, A. Gjedde, R. N. Gunn, J. Holden, S. Houle, S.-C. Huang, M. Ichise, H. Iida, H. Ito, Y. Kimura, R. A. Koeppe, G. M. Knudsen, J. Knuuti, A. A. Lammertsma, M. Laruelle, J. Logan, R. P. Maguire, M. A. Mintun, E. D. Morris, R. Parsey, J. C. Price, M. Slifstein, V. Sossi, T. Suhara, J. R. Votaw, D. F. Wong, R. E. Carson, Consensus nomenclature for in vivo imaging of reversibly binding radioligands. *J. Cereb. Blood Flow Metab.* **27**, 1533–1539 (2007).
39. M. Gillard, B. Fuks, P. Michel, P. Vertongen, R. Massingham, P. Chatelain, Binding characteristics of [^{3}H]ucb 30889 to levetiracetam binding sites in rat brain. *Eur. J. Pharmacol.* **478**, 1–9 (2003).
40. M. Gillard, B. Fuks, K. Leclercq, A. Matagne, Binding characteristics of brivaracetam, a selective, high affinity SV2A ligand in rat, mouse and human brain: Relationship to anti-convulsant properties. *Eur. J. Pharmacol.* **664**, 36–44 (2011).
41. L. Farde, H. Hall, E. Ehrin, G. Sedvall, Quantitative analysis of D2 dopamine receptor binding in the living human brain by PET. *Science* **231**, 258–261 (1986).
42. L. Alonso-Nanclares, J. Gonzalez-Soriano, J. R. Rodriguez, J. DeFelipe, Gender differences in human cortical synaptic density. *Proc. Natl. Acad. Sci. U.S.A.* **105**, 14615–14619 (2008).
43. S. O. Rizzoli, W. J. Betz, Synaptic vesicle pools. *Nat. Rev. Neurosci.* **6**, 57–69 (2005).
44. I. Savic, M. Ingvar, S. Stone-Elander, Comparison of [^{11}C]flumazenil and [^{18}F]FDG as PET markers of epileptic foci. *J. Neurol. Neurosurg. Psychiatry* **56**, 615–621 (1993).
45. E. J. Hoffman, S.-C. Huang, M. E. Phelps, Quantitation in positron emission computed tomography: 1. Effect of object size. *J. Comput. Assist. Tomogr.* **3**, 299–308 (1979).
46. C. R. Overk, E. Masliah, Pathogenesis of synaptic degeneration in Alzheimer's disease and Lewy body disease. *Biochem. Pharmacol.* **88**, 508–516 (2014).
47. M. Naganawa, R. N. Waterhouse, N. B. Nabulsi, S. F. Lin, D. Labaree, J. Ropchan, S. Tarabar, N. DeMartinis, A. Ogden, A. Banerjee, Y. Huang, R. E. Carson, First in human assessment of the novel PDE2A PET radiotracer 18F-PF-05270430. *J. Nucl. Med.* jnumed.115.166850 (2016).

48. J.-D. Gallezot, M.-Q. Zheng, K. Lim, S.-f. Lin, D. Labaree, D. Matuskey, Y. Huang, Y.-S. Ding, R. E. Carson, R. T. Mallison, Parametric imaging and test–retest variability of $[^{11}C]$-(+)-PHNO binding to D_2/D_3 dopamine receptors in humans on the high-resolution research tomograph PET scanner. *J. Nucl. Med.* **55**, 960–966 (2014).
49. M. Nord, S. J. Finnema, M. Schain, C. Halldin, L. Farde, Test–retest reliability of $[^{11}C]$AZ10419369 binding to 5-HT_{1B} receptors in human brain. *Eur. J. Nucl. Med. Mol. Imaging* **41**, 301–307 (2014).
50. R. E. Carson, M. A. Channing, R. G. Blasberg, B. B. Dunn, R. M. Cohen, K. C. Rice, P. Herscovitch, Comparison of bolus and infusion methods for receptor quantitation: Application to $[^{18}F]$cyclofoxy and positron emission tomography. *J. Cereb. Blood Flow Metab.* **13**, 24–42 (1993).
51. R. E. Carson, W. C. Barker, J.-S. Liow, C. A. Johnson, Design of a motion-compensation OSEM list-mode algorithm for resolution-recovery reconstruction for the HRRT. *IEEE Nucl. Sci. Symp. Conf. Rec.* **5**, 3281–3285 (2003).
52. X. Jin, C. Chan, T. Mulnix, V. Panin, M. E. Casey, C. Liu, R. E. Carson, List-mode reconstruction for the Biograph mCT with physics modeling and event-by-event motion correction. *Phys. Med. Biol.* **58**, 5567–5591 (2013).
53. X. Papademetris, M. P. Jackowski, N. Rajeevan, M. DiStasio, H. Okuda, R. T. Constable, L. H. Staib, BioImage Suite: An integrated medical image analysis suite. *Insight J.* **2006**, 209 (2006).
54. C. M. Sandiego, D. Weinzimmer, R. E. Carson, Optimization of PET–MR registrations for nonhuman primates using mutual information measures: A multi-transform method (MTM). *Neuroimage* **64**, 571–581 (2013).
55. J. Hilton, F. Yokoi, R. F. Dannals, H. T. Ravert, Z. Szabo, D. F. Wong, Column-switching HPLC for the analysis of plasma in PET imaging studies. *Nucl. Med. Biol.* **27**, 627–630 (2000).
56. M. Gillard, P. Chatelain, B. Fuks, Binding characteristics of levetiracetam to synaptic vesicle protein 2A (SV2A) in human brain and in CHO cells expressing the human recombinant protein. *Eur. J. Pharmacol.* **536**, 102–108 (2006).
57. P. K. Smith, R. I. Krohn, G. T. Hermanson, A. K. Mallia, F. H. Gartner, M. D. Provenzano, E. K. Fujimoto, N. M. Goeke, B. J. Olson, D. C. Klenk, Measurement of protein using bicinchoninic acid. *Anal. Biochem.* **150**, 76–85 (1985).

Acknowledgments: We thank the staff of the Yale PET Center for their expert assistance. **Funding:** Research support was provided by the Swebilius Foundation and UCB Pharma. S.J.F. was supported by an international postdoctoral grant from the Swedish Research Council. This publication was made possible by Clinical and Translational Science Award grant no. UL1 TR000142 from the National Center for Advancing Translational Science, a component of the NIH. Its contents are solely the responsibility of the authors and do not necessarily represent the official view of the NIH. **Author contributions:** S.J.F. designed the study and performed the experiments, data analysis, and manuscript preparation. N.B.N. performed the PET experiments and manuscript preparation. T.E. performed the Western blot and confocal microscopy experiments and manuscript preparation. K.D. recruited epilepsy patients and performed PET image interpretation and manuscript preparation. S.-f.L. performed the homogenate binding studies and PET experiments. M.-K.C. performed ex vivo and PET experiments and manuscript preparation. R.D. performed the Western blot and confocal microscopy experiments. D.M. recruited healthy control subjects and performed the PET experiments. E.B. performed homogenate binding studies and PET experiments. D.H. performed the baboon ex vivo and PET experiment. D.D.S. designed the PET study and facilitated patient selection. J.M. designed the PET experiments. J.H. designed the PET experiments and performed manuscript preparation. Y.H. designed and performed the PET experiments and manuscript preparation. R.E.C. designed the study and performed data analysis and manuscript preparation. All authors reviewed and approved the final version of this manuscript. **Competing interests:** J.M. and J.H. were full-time employees of UCB Pharma at the time this work was planned, conducted, and analyzed. J.H. is currently a full-time employee of Denali Therapeutics. All other authors declare no competing financial interests. **Data and materials availability:** All data are shown, and all materials are commercially available.

Submitted 10 March 2016
Accepted 24 June 2016
Published 20 July 2016
10.1126/scitranslmed.aaf6667

Citation: S. J. Finnema, N. B. Nabulsi, T. Eid, K. Detyniecki, S.-f. Lin, M.-K. Chen, R. Dhaher, D. Matuskey, E. Baum, D. Holden, D. D. Spencer, J. Mercier, J. Hannestad, Y. Huang, R. E. Carson, Imaging synaptic density in the living human brain. *Sci. Transl. Med.* **8**, 348ra96 (2016).

Science Translational Medicine

Imaging synaptic density in the living human brain

Sjoerd J. Finnema, Nabeel B. Nabulsi, Tore Eid, Kamil Detyniecki, Shu-fei Lin, Ming-Kai Chen, Roni Dhaher, David Matuskey, Evan Baum, Daniel Holden, Dennis D. Spencer, Joël Mercier, Jonas Hannestad, Yiyun Huang and Richard E. Carson

Sci Transl Med **8**, 348ra96348ra96.
DOI: 10.1126/scitranslmed.aaf6667

Seeing synapses

When synapses "fire," information is transmitted from one neuron to another. Although many neurological and psychiatric diseases are characterized by misfiring synapses, there is currently no way to visualize healthy or aberrant neuronal connections in the living brain––tissues would need to be sampled, which is an invasive and often unwanted procedure. Finnema and colleagues developed a noninvasive approach to "see" human synapses by using an imaging agent that targets the synaptic vesicle glycoprotein 2A (SV2A). PET imaging allowed the a uthors to visualize synaptic density in both healthy and epileptic human brains in living patients. In the brains with epilepsy, synaptic density was asymmetric––consistent with damage to certain brain regions. This method opens doors to routine monitoring of the brain in patients with various neurological diseases, where synaptic loss or dynamic changes in density could provide clues to prognosis.